Romanian Reports in Physics **XX**, XYZ (2021)

EYE TUMOR TISSUES IMAGING WITH WHITE LIGHT DIFFRACTION PHASE MICROSCOPY

V. NASTASA[1,†], ADRIANA SMARANDACHE[2,*,†], RUXANDRA A. PIRVULESCU[3,4,†], I.R. ANDREI[2], G. SIMION[4], G. POPESCU[5], M.L. PASCU[2,6]

[1] Extreme Light Infrastructure - Nuclear Physics ELI-NP, "Horia Hulubei" National Institute for Physics and Nuclear Engineering IFIN-HH, 077125 Magurele, Romania;
E-mail: viorel.nastasa@eli-np.ro
[2] National Institute for Laser, Plasma and Radiation Physics, 077125 Magurele, Romania;
E-mails: adriana.smarandache@inflpr.ro; ionut.andrei@inflpr.ro; mihai.pascu@inflpr.ro
[3] University of Medicine and Pharmacy "Carol Davila", 020022 Bucharest, Romania;
E-mail: ruxandrapascu78@gmail.com
[4] Emergency University Hospital Bucharest, 050098 Bucharest, Romania;
E-mail: george.simion2007@yahoo.com
[5] Beckman Institute for Advanced Science and Technology, University of Illinois at Urbana-Champaign, Urbana, 61801, Illinois, USA;
E-mail: gpopescu@illinois.edu
[6] Physics Faculty, University of Bucharest

[*]Correspondence: mihai.pascu@inflpr.ro;
[†] First authors who contributed equally to this work.

Received July 29, 2021

Abstract. In the current context of histopathology, where the gold standard remains the manual investigation of stained tissues, development of new sensitive methods for early diagnosis of diseases is necessary. White light diffraction phase microscopy, may answer this challenge by detecting very small variations of refractive indexes in biological specimens. Eye tissue samples images were acquired by conventional microscopy, and by white light diffraction phase microscopy technique. A comparative histological analysis was performed to evidence the characteristics of biological structures. Quantitative images with increased contrast of some cellular structures were obtained using white light diffraction phase microscopy.

Key words: eye tumor; white light diffraction phase microscopy; quantitative phase imaging; phase map; refractive index.

1. INTRODUCTION

Finding ways to diagnose and treat cancer in early stage is of high importance since its status strongly influences the surviving chance of the patient. One of the main directions in diagnostic pathology is to develop new methods that can provide accurate results at lower costs. Despite its four-century-long history, optical microscopy continues to be the current state of the art in histopathology [1], where

several µm thick tissue slices are optically evaluated under a microscope. However, while stains offer high-contrast imaging with molecular specificity, the histological analysis requires sample preparation and is often qualitative and subjective, as it involves human observation by an experienced pathologist. On the other hand, the stain chemicals can introduce variability and errors.

In the last decades, it has been found that by combining holography and microscopy, highly sensitive measurements capable of detecting very small refractive index (RI) variations of thin biological specimens can be performed [2]. Afterwards, efforts were made to develop full-field quantitative phase imaging (QPI) methods, in which the phase map across a field of view is retrieved simultaneously. Because the optical pathlength (or phase) contains information about both the sample RI and thickness, QPI has been used to provide measurements of red blood cells (RBC) volumes [3], cell dry mass [4,5] and dynamics [6], cell tomography [7,8], and tissue scattering [9,10]. As a QPI technique, diffraction phase microscopy (DPM) has been widely used since its invention as a stable and high-throughput method for extracting the complex image field associated with an object and, therefore, its phase [11]. Furthermore, the off-axis geometry of white light diffraction phase microscopy (wDPM) which combines the benefits of temporal sensitivity associated with DPM and the spatial sensitivity associated with white light illumination, allows single-shot measurements and thus permits rapid phenomena analysis. More important advantages originate in its common-path architecture, which ensures phase stability against noise and allows achieving high temporal phase sensitivity [12]. The quantitative imaging capability of wDPM was demonstrated by the first imaging of live RBCs [13]. Also, a quantitative phase image of HeLa cell (ATCC, CCL-2), a human cervical epithelial constituent obtained out of a cell line, revealed cell structure components, such as nucleoli [14].

The goal of this paper is to demonstrate, for the first time to our knowledge, the ability of wDPM to provide quality imaging of eye tissues samples. We present a comparison between conventional microscopy and wDPM data obtained on samples excised from different patients and regions of the eye tissues. We also emphasize the boost in contrast and quantitative features provided by QPI. We anticipate that this study will stimulate further research in the area of eye pathology investigated through QPI techniques, which is currently unexplored.

2. MATERIALS AND METHODS

Different ocular tumor tissues explored in this paper were surgically harvested while maintaining safety margins. These samples were sent to

histopathological examination in the first instance. All patients out of whom samples were harvested and used for this paper signed an informed consent in accordance with the Declaration of Helsinki [15]. The Ethics Committee approved the study at the Emergency University Hospital in Bucharest, Romania (protocol nr. 50706 / 08.10.2020). The processing of the biopsy material was carried out according to the protocol in several stages: fixation, dehydration, clearing, wax infiltration, embedding, sectioning and staining.

Samples of eyeball fragments consisting of 3-4 μm thick slices stained with the usual dye hematoxylin and eosin (H&E) and Verhoeff-Van Gieson (VVG) were first analyzed by conventional microscopy using an inverted microscope (Axio Observer 7, Zeiss, Germany) with the objective 20x having numerical aperture (NA) 0.4. The same samples were subsequently analyzed by wDPM method, using the corresponding set-up described in detail by Kim & al. [16]. The wDPM module installed at the exit port of the inverted microscope limits the temporal phase noise and increases the sensitivity for the measurement due to its common-path geometry. By using QPI for tissue analysis, a map of optical densities can be obtained, which in turn may be correlated with other information retrieved from the observed sample for a more accurate diagnosis. Similar methods are presented in the literature, where a dependence of RI variation on tissue nature (benign/malignant) is shown [17–19].

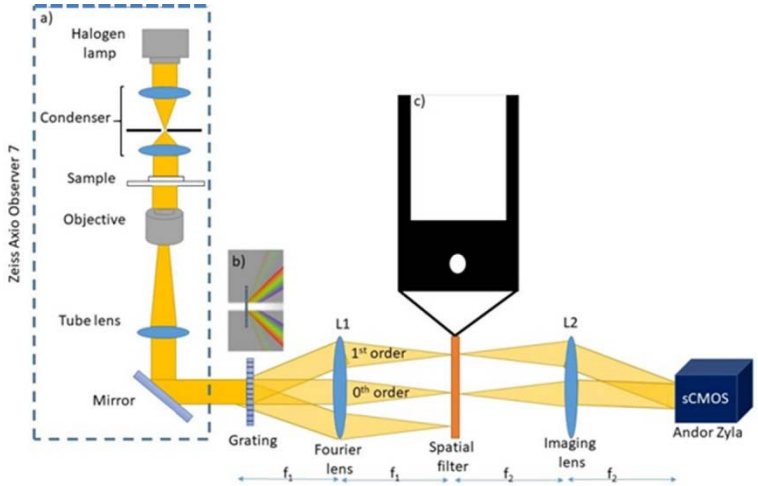

Fig. 1 – Experimental set-up. A transmission grating was placed at the image plane of an inverted microscope, followed by a 4f imaging system. The diffraction orders are collected with a Fourier lens, filtered by a spatial filter, and sent through an imaging lens to the (sCMOS, Andor Zyla, Oxford Instruments) camera.

The experimental set-up used for this study is shown in Fig. 1 and consists of an inverted microscope (Axio Observer 7, Zeiss, Germany) equipped with a LED

light source and the interferometric system coupled at one of the microscope's exit ports. To ensure a spatially coherent illumination field, we closed the condenser aperture of the microscope down to 0.09 NA. The intensity signal obtained from the microscope is passed through the transmission diffraction grating (110 grooves/mm) that generates several diffraction orders making available copies of the incident image spread at different angles. The attained diffraction orders are focused with a lens onto a spatial filter placed in the Fourier plane of lens L_1 that allows passing of a low-pass filtered 0^{th} and the 1^{st} diffraction orders. The LED lamp, used as an uncoherent white light source with low temporal coherence, allows us to minimize the speckle noise that can affect the phase imaging system's spatial sensitivity.

For a microscope operating in transmission mode, the resolution is given by Abbe's formula [20]:

$$\Delta\rho = \frac{1.22\lambda}{NA_{obj}+NA_{con}} \quad (1)$$

where: Δρ represents the diffraction spot radius or the distance from the peak to the first zero of the Airy patterns; λ is the wavelength of light; NA_{obj} and NA_{con} are the objective and condenser numerical apertures. The resolution of the wDPM system used in this study, calculated according to the Rayleigh criterion, is thus approximately 1.35 μm.

If proper sampling is used, a quantitative phase map can be obtained *via* a Hilbert transform, as described in [13]. The phase reconstruction procedure uses a calibration background image, which is subsequently subtracted in order to generate a high contrast image of the specimen, free of instrument imperfections and specimen-unrelated light patterns. A Fourier transform is applied on the sample's raw interference image, generating the power spectrum of the image. To obtain a phase map of the sample, one of the diffraction orders attained in the power spectrum is selected and moved to the image frequency spectrum center. An inverse Fourier transform is applied to bring it back into the space domain, thus, generating a phase map of the specimen [21].

Quantifying optical path-length shifts across the specimen offers a new dimension to imaging, which reports on both the refractive index and thickness distribution with very high accuracy. The corresponding mathematical relationship between these values is expressed by equation (2):

$$\Delta\phi = knL \quad (2)$$

where $\Delta\phi$ is the phase shift of the incident light, $k = 2\pi/\lambda$ and assuming negligible refraction at the surface, n is RI of the medium having thickness L, and λ is the wavelength of the optical radiation. When moving from one medium of refractive index n_1 to another of refractive index n_2, this relation becomes:

$$\Delta\phi = k(n_1+n_2)L \quad (3)$$

It was shown that quantitative phase imaging of thin biological slices can be used to spatially map the tissue in terms of its scattering properties [22]. More precisely, mathematical relationships were derived between the phase map $\phi(r)$ associated with a tissue slice of thickness $L<<l_s$, and scattering parameters of the bulk: l_s as the scattering mean free path, and g, which can be defined by the average cosine of the field transmitted through a slice of thickness l_s. Thus, the expression of the scattering mean free path is written as:

$$l_s = \frac{L}{\langle \Delta\phi^2(r) \rangle_r} \quad (4)$$

and the anisotropy factor is:

$$g = 1 - \left(\frac{l_s}{L}\right)^2 \frac{\langle |\nabla[\phi(r)]|^2 \rangle_r}{2k_0^2} \quad (5)$$

where L is the thickness of the tissue slice; l_s, scattering mean free path; k_0 the incident wave vector; $|\nabla[\phi(r)]|^2$ the spatial variance of ϕ.

For the physical interpretation, the l_s–ϕ relationship simply shows that the attenuation due to scattering is stronger (l_s shorter) as the tissue roughness (variance) is larger, meaning that the more inhomogeneous is the tissue, the stronger is the scattering. On the other hand, the g–ϕ formula contains the gradient of the phase. The higher the gradient variance, the higher the probability for large scattering angles, *i.e.* smaller g value. Accordingly, a thin tissue slice acts as a complicated phase grating, which is characterized by a certain diffraction efficiency controlled by l_s and average diffraction angle, determined by g [22].

3. RESULTS AND DISCUSSIONS

The selected samples were studied in brightfield (BF), phase contrast (PH), and wDPM using a 20x/0.4 NA objective of the microscope. Thin biological samples have weak absorption/scattering of light and, therefore, are transparent in white light.

Histologically, the ciliary body consists of the ciliary epithelium, the stroma and muscle, as well as the supraciliary space. The ciliary epithelium consists of a non-pigmented inner layer covered by an outer pigmented one. The stroma is composed of collagen layers, ciliary muscles and cells (fibroblasts, melanocytes, scattered mast cells, vessels, and nerves). The thin collagen layer that separates the ciliary body from the sclera represents the supraciliary space [23].

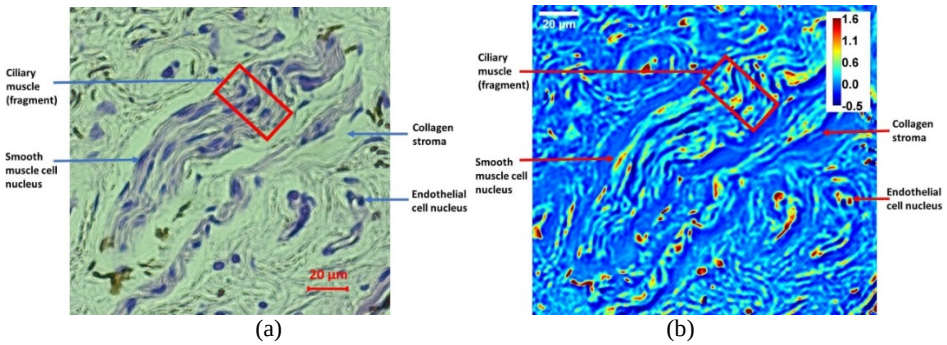

(a) (b)

Fig. 2 – Ciliary body with its muscles – H&E staining: a) BF image taken with the inverted microscope (20x/0.4NA objective); b) Phase map obtained using a wDPM system, where color bar represents the phase in radians, which corresponds to the optical pathlength through the specimen; blue colors are linked with lower optical pathlengths, and therefore lower RI, and dark brown color relates to highest optical pathlength (highest RI).

The histological analysis of the sample presented in Fig. 2(a) shows a ciliary pigmented epithelium with lax subepithelial stroma that contains a bundle of ciliary smooth muscle. The same nuclei can be observed in the phase map highlighted in Fig. 2(b) as presenting high RI distributed on a blue background; the cytoplasm of the smooth muscle cells is evidenced on a light blue background, indicative of low RI.

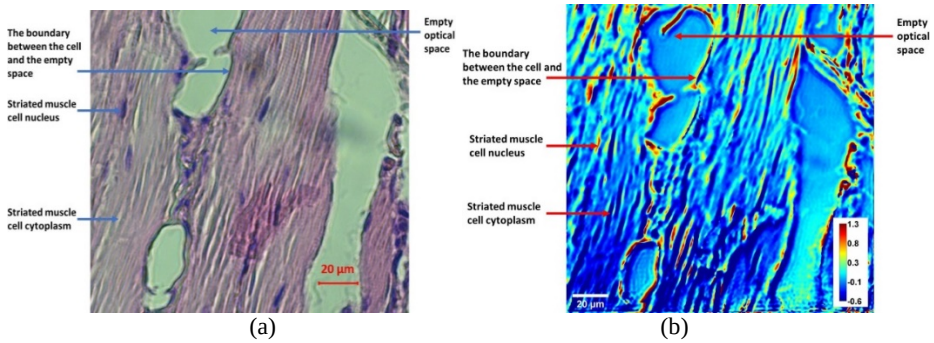

(a) (b)

Fig. 3 – Skeletal muscle fibers – H&E staining: a) BF image taken with the inverted microscope (20X/0.4NA objective); b) Phase map obtained using a wDPM system, where color bar represents the phase in radians, which corresponds to the optical pathlength through the specimen; blue colors correspond to lower optical pathlengths, and therefore lower RI, and dark brown color relates to highest optical pathlength (highest RI).

The histological analysis in Fig. 3(a) shows muscle-skeletal fibers in longitudinal section with empty optical spaces between fibers. The membrane of these fibers appears yellow in the phase map - Fig. 3(b). The muscle cells' nuclei have high RI, highlighted in a brown color that is surrounded by yellow contour.

In Fig. 4(a), a squamous non-keratinized epithelium may be seen, as well as subepithelial stroma with fibrocyte cells and rare capillary vessels. The nuclei of the fibrocyte and endothelial cells with high RIs have brown color surrounded by a fine yellow contour, as shown in Fig. 4(c). Also, the limit between the squamous epithelium and the empty optical space appears linear and brown with yellow margins.

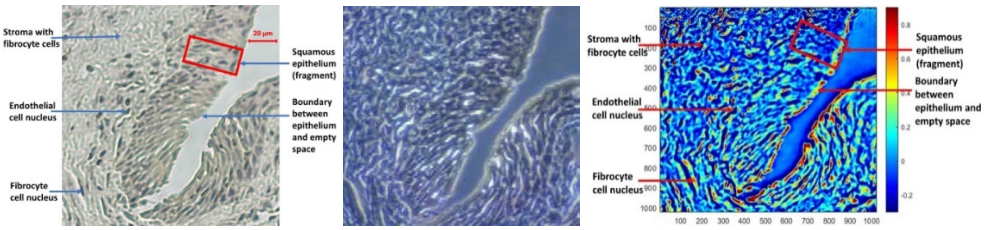

(a) (b) (c)

Fig. 4 – Conjunctival epithelium (eyelid) - VVG staining: a) BF image taken with the inverted microscope (20x/0.4NA objective); (b) phase contrast (PH) and (c) wDPM image of ophthalmic tissue sample. Color bar in (c) represents phase in radians, which corresponds to the optical pathlength through the specimen: blue colors correspond to lower optical pathlengths, and therefore lower RI, and dark brown color indicates the highest optical pathlength (highest RI).

In optical microscopy, the raw biological samples are usually optically transparent, which leads to low-contrast images when using a conventional microscope. However, even if the sample does not absorb light, it shows a distribution of refractive index that perturbs the wave front which can be used as an intrinsic source of contrast [25]. One may observe that, due to its RI sensitivity, wDPM is capable of highlighting tissue structures and features that are less visible in BF, an absorption-based contrast method. A particular attention should be devoted to the imaging of collagen fibers since their composition, orientation and alignment in the stroma of adjacent tumors may be indicative about cancer growth and metastasis [24].

Despite its significant advances, biomedical optical imaging continues to be an active research domain, aiming to go beyond the spatial and temporal resolution achieved so far. Penetration depth, contrast, molecular specificity, and quantitative possibilities represent characteristics to be improved. For example, common-path interferometry replaced traditional interferometry for better stability and sensitivity [11, 25, 26]. Low temporal coherence illumination methods significantly improve image resolution when suppressing speckles [27]. Three-dimensional information of the specimen is accessible by measuring the phase across multiple angles of the illumination or axial specimen positions [28]. An equivalent approach proposed by Merola *et al.* is fixing the illumination direction while rotating the sample to obtain phase maps from different viewing angles [29]. Lens-free holography method is

also used to obtain tomographic information on a chip by combining with multiple illumination angles [30]. However, imaging optically thick, multiple scattering specimens is still challenging for any optical method, including QPI. The fundamental obstacle is that multiple scattering generates an incoherent background, which ultimately degrades the image contrast. An imaging method dedicated to obtain images of thick specimens must include a mechanism to subdue the multiple scattering backgrounds and exhibit strong sectioning to suppress the out-of-focus light. To overcome these challenges, it was introduced the gradient light interference microscopy (GLIM), which combines differential interference contrast microscopy with low-coherence interferometry and holography [31]. Likewise, as a label-free imaging modality, QPI techniques lack chemical specificity. However, recently, it has been shown that such molecular specificity can be retrieved via deep-learning algorithms, thus removing the need for chemical stains [32–35]. All the recent works predict that the combination of QPI and computation will associate the benefits of label-free, quantitative imaging with specificity, thus, opening new frontiers in histopathology.

4. CONCLUSIONS

The obtained data show that QPI and, particularly, wDPM can be a valuable tool for histopathological examination of tissues. Due to its sensitivity to the specimen's intrinsic refractive properties, wDPM is capable of highlighting histopathology details that are not available through standard methods. The side-by-side comparison of hematoxylin and eosin and Verhoeff-Van Gieson-stained microscopic images and those obtained by wDPM shows that the increased interferometric contrast provides an objective measure of structural details.

We showed that wDPM could reveal cellular and subcellular structures in transparent tissue slices based on the refractive index distribution. Generally, the images of the fibrocyte, endothelial, muscle, and RBC cells nuclei appear colored as brownish with fine yellow borders in the phase maps obtained with QPI system, corresponding to a high refractive index. The cytoplasm of the smooth muscle cells, with a low refraction index, appears light blue, and the limit between cells and optical empty spaces has a linear shape with brown or yellow color. In both, bright field method and in wDPM, the nuclei are easily identified. Nevertheless, small visual differences are observed between the two methods due to the specific measurement mode in wDPM. However, more detailed quantitative information can be obtained with wDPM since the phase map corresponds to optical pathlengths' differences through samples. In this line, special attention deserves to

be paid to connective anatomical elements considering that collagen fiber alignment and orientation are potential markers for patient prognosis.

In order to use this type of image for diagnostics purposes, it is necessary to introduce new criteria and standards for the interpretation of the shapes and colors based on the refractive index distribution of different biological structures. To do this, we must analyze more complex lesion categories and initiate a library of characteristic quantitative physical parameters. The method may also be useful in some organ diseases where incipient fibrosis is an issue, not necessarily distinguishing between benign and malignant tissues.

Acknowledgements. This research was funded by grants of the MCID and UEFISCDI, specifically, projects PN-III-P2-2.1-PED-2016-0446, PN-III-P2-2.1-PED-2019-1264, and Program-Core research-development, ctr. no. 16N /08.02.2019. Gabriel Popescu was supported by NIH (USA), through R01GM129709 and R01CA238191; R43GM133280-01.

The authors are grateful to Dr. H. Majeed and Dr. M. Kandel for their help with the implementation of the wDPM system, as well as to Prof. K. Spohr for manuscript's check and correction.

REFERENCES

1. Milestones in light microscopy, Nat. Cell Biol. **11**, 1165–1165 (2009).
2. K. Creath, V Phase-Measurement Interferometry Techniques, in *Progress in Optics*, (Elsevier, 1988).
3. G. Popescu, T. Ikeda, C. Best, K. Badizadegan, R. R. Dasari, and M. S. Feld, J. Biomed. Opt. **10**, 060503 (2005).
4. G. Popescu, Y. Park, N. Lue, C. Best-Popescu, L. Deflores, R. R. Dasari, M. S. Feld, and K. Badizadegan, Am. J. Physiol.-Cell Physiol. **295**, C538–C544 (2008).
5. M. Mir, Z. Wang, Z. Shen, M. Bednarz, R. Bashir, I. Golding, S. G. Prasanth, and G. Popescu, Proc. Natl. Acad. Sci. **108**, 13124–13129 (2011).
6. R. Wang, Z. Wang, J. Leigh, N. Sobh, L. Millet, M. U. Gillette, A. J. Levine, and G. Popescu, J. Phys. Condens. Matter Inst. Phys. J. **23**, 374107 (2011).
7. F. Charrière, N. Pavillon, T. Colomb, C. Depeursinge, T. J. Heger, E. A. D. Mitchell, P. Marquet, and B. Rappaz, Opt. Express **14**, 7005–7013 (2006).
8. Z. Wang, D. L. Marks, P. S. Carney, L. J. Millet, M. U. Gillette, A. Mihi, P. V. Braun, Z. Shen, S. G. Prasanth, and G. Popescu, Opt. Express **19**, 19907–19918 (2011).
9. Z. Wang, G. Popescu, K. V. Tangella, and A. Balla, J. Biomed. Opt. **16**, 116017 (2011).
10. A. Bokemeyer, P. R. Tepasse, L. Quill, P. Lenz, E. Rijcken, M. Vieth, N. Ding, S. Ketelhut, F. Rieder, B. Kemper, and D. Bettenworth, Sci. Rep. **9**, 19388 (2019).
11. B. Bhaduri, C. Edwards, H. Pham, R. Zhou, T. H. Nguyen, L. L. Goddard, and G. Popescu, Adv. Opt. Photonics **6**, 57–119 (2014).
12. M. Shan, M. E. Kandel, H. Majeed, V. Nastasa, and G. Popescu, Opt. Express **24**, 29033–29039 (2016).
13. T. Ikeda, G. Popescu, R. R. Dasari, and M. S. Feld, Opt. Lett. **30**, 1165–1167 (2005).
14. B. Bhaduri, H. Pham, M. Mir, and G. Popescu, Opt. Lett. **37**, 1094–1096 (2012).
15. WMA - The World Medical Association-WMA Declaration of Helsinki – Ethical Principles for Medical Research Involving Human Subjects, https://www.wma.net/policies-post/wma-declaration-of-helsinki-ethical-principles-for-medical-research-involving-human-subjects/.

16. T. Kim, R. Zhou, M. Mir, S. D. Babacan, P. S. Carney, L. L. Goddard, and G. Popescu, Nat. Photonics **8**, 256–263 (2014).
17. B. Kemper, A. Bauwens, A. Vollmer, S. Ketelhut, P. Langehanenberg, J. Müthing, H. Karch, and G. von Bally, J. Biomed. Opt. **15**, 036009 (2010).
18. N. T. Shaked, T. M. Newpher, M. D. Ehlers, and A. Wax, Appl. Opt. **49**, 2872 (2010).
19. N. Lue, J. Bewersdorf, M. D. Lessard, K. Badizadegan, R. R. Dasari, M. S. Feld, and G. Popescu, Opt. Lett. **32**, 3522 (2007).
20. B. Masters, *Superresolution Optical Microscopy: The Quest for Enhanced Resolution and Contrast* (Springer International Publishing, 2020).
21. C. Hu, R. Sam, M. Shan, V. Nastasa, M. Wang, T. Kim, M. Gillette, P. Sengupta, and G. Popescu, J. Biophotonics **12**, e201800269 (2019).
22. Z. Wang, H. Ding, and G. Popescu, Opt. Lett. **36**, 1215–1217 (2011).
23. F. A. Marigo and P. T. Finger, Surv. Ophthalmol. **48**, 569–593 (2003).
24. H. Majeed, C. Okoro, A. Kajdacsy-Balla, K. C. Toussaint, and G. Popescu, J. Biomed. Opt. **22**, 046004 (2017).
25. M. E. Kandel, C. Hu, G. Naseri Kouzehgarani, E. Min, K. M. Sullivan, H. Kong, J. M. Li, D. N. Robson, M. U. Gillette, C. Best-Popescu, and G. Popescu, Nat. Commun. **10**, 4691 (2019).
26. M. E. Kandel, K. W. Teng, P. R. Selvin, and G. Popescu, ACS Nano **11**, 647–655 (2017).
27. B. Bhaduri, H. Pham, M. Mir, and G. Popescu, Opt. Lett. **37**, 1094–1096 (2012).
28. T. S. Ralston, D. L. Marks, P. Scott Carney, and S. A. Boppart, "Interferometric synthetic aperture microscopy," Nat. Phys. **3**, 129–134 (2007).
29. F. Merola, P. Memmolo, L. Miccio, R. Savoia, M. Mugnano, A. Fontana, G. D'Ippolito, A. Sardo, A. Iolascon, A. Gambale, and P. Ferraro, Light Sci. Appl. **6**, e16241–e16241 (2017).
30. S. O. Isikman, W. Bishara, H. Zhu, and A. Ozcan, Appl. Phys. Lett. **98**, 161109 (2011).
31. T. H. Nguyen, M. E. Kandel, M. Rubessa, M. B. Wheeler, and G. Popescu, Nat. Commun. **8**, 210 (2017).
32. Y. A. Jnr, J. Med. Artif. Intell. **3**, (2020).
33. Y. Jo, H. Cho, S. Y. Lee, G. Choi, G. Kim, H. Min, and Y. Park, IEEE Journal of Selected Topics in Quantum Electronics, **25**, 1-14, (2019).
34. Y. Rivenson, T. Liu, Z. Wei, Y. Zhang, K. de Haan, and A. Ozcan, Light Sci. Appl. **8**, 23 (2019).
35. C. L. Chen, A. Mahjoubfar, L.-C. Tai, I. K. Blaby, A. Huang, K. R. Niazi, and B. Jalali, Sci. Rep. **6**, 21471 (2016).